REINFORCED CONCRETE EXTERIOR WIDE AND CONVENTIONAL BEAM-COLUMN JOINTS UNDER EARTHQUAKE-TYPE LOADING

H. Behnam[(1)], J.S. Kuang[(2)], Q. Huang[(3)]

[(1)] *PhD Candidate, Hong Kong University of Science and Technology, Hong Kong. hbehnam@ust.hk*
[(2)] *Professor, Hong Kong University of Science and Technology, Hong Kong. cejkuang@ust.hk*
[(3)] *Associate Professor, Huaqiao University, Xiamen, China. huangqx@hqu.edu.cn*

Abstract

The seismic behaviour of reinforced concrete (RC) exterior wide and conventional beam-column joints was investigated through experimental and computational simulation. Two full-scale specimens were designed, constructed and tested under reversed quasi-static cyclic loading. Specimens had the beam-width to column-width ratios of 1 and 1.5, representing the conventional and wide beam-column connections and were designed in conformance with ACI 318-14 and ACI 352-R02. Seismic performance of the connections was evaluated based on the results obtained from the experiments, such as crack pattern, hysteresis response, ductility ratio, and the strain profiles of the longitudinal and transverse reinforcement of specimens. The results indicated that both specimens were capable of supporting the complete formation of beam plastic hinges with no major cracks in the joint region. Both specimens attained their negative and positive design strengths at a drift level of 1.1%. Computer simulations with a 3D nonlinear finite element model (FEM) using ABAQUS were carried out. Two sets of results from the experiment and computer simulation were compared, and good agreement was found. The calibrated FEM was then used to investigate the role of the transverse reinforcement in the joint region. Experimental and numerical verification showed that both conventional and wide beam-column joints designed with the current design procedure recommended in ACI can perform well in carrying the horizontal lateral loads. A parametric study using FEM indicated that minimum amount of the joint transverse reinforcement recommended by ACI code is an acceptable limit in both conventional and wide beam-column joint. Providing additional joint transverse reinforcement will not increase the joint shear strength, but it causes difficulties in construction of the wide beam-column connections.

Keywords: wide beam-column joint; computational simulation; full-scale specimens; cyclic loading; hysteresis response.

1. Introduction

Long-spans and heavily loaded reinforced concrete moment-resisting frame structures (RCMRF) are frequently built with wide and shallow beams joining all of the columns. The wide beam structural floor system offers several advantages over conventional framing systems because of the benefits in architectural planning, low storey height, simplified formwork, fast construction and reduced overall cost of the project. However, potential advantages and applications of the wide beam system as a lateral load-resisting structure are often ignored due to the lack of understanding of the performance of these structures. In fact, the resistance of the beam-column connections in this structural system against lateral earthquake loading is the major concern of structural engineers. The exterior wide beam-column connections are not only susceptible to joint shear failure, but also they are highly vulnerable to failure of the spandrel (transverse) beam in torsion. The wide beam-column connections can be thought of as a special case between a conventional beam-column connection and slab-column connections [1-2]. Although extensive experimental and numerical studies have been conducted on the seismic performance of both conventional beam-column joints and slab-column joints [3-7], there are only a few specific types of research available about the behaviour of wide-beam-column joints.

From the published literature, a limited number of experimental studies have been carried out on the wide beam-column connection [8-14]. These experimental studies were focused on the different aspects of the connection. Gentry and Wight tested four exterior 3/4-scale wide beam-column joints. It was found that wide beam-column joints performed well if design parameters were carefully controlled. The main parameters in this investigation were beam to column width ratio and amount of beam reinforcement not placed in the joint core [8]. Test results by LaFave and Wight [9] showed that these joints with a proper design possessed adequate strength and deformation capacity. Recent experimental investigation on four full-scale wide and conventional exterior and interior beam-column connections with continuous column was carried out by Fadwa et al. [13] showed that the hysteresis response and total energy dissipation capacity of the wide beams were better than those of conventional beams.

From the literature review, it can be noted that most of the tested specimens had a beam width to column ratio larger than two, while in practice, sometimes the beam is just slightly wider than the framed column. Hence, more research is needed to clarify the behaviour of the connection in which the beam is slightly wider than the framing column (beam width ratio smaller than two). To this end, an experimental research was carried out on two full-scale specimens to evaluate and compare the seismic performance of the wide and conventional beam-column connections. Regarding the specific nature of the tested specimens, only major parameters such as beam width and reinforcement were changed in tested specimens. In addition, the finite element model (FEM) was developed to supplement experimental data and to provide insights into the structural behaviour of the wide beam-column joint.

2. Experimental Programme

Two full-scale exterior RC beam-column connections were designed, constructed, and tested under reversed quasi-static cyclic loading. The specimens were designed and detailed in conformance with ACI 318-14 requirements and its recommendations (ACI 352R-02) for designing RC structures in high seismic zones. Specimen with beam width to column width ratio of one (conventional joint) was labelled as S1-BC1. Specimen with beam width to column width ratio of 1.5 (wide beam-column joint) was named S2-BC1.5. The specimens representing a portion of the framing system were obtained by terminating the beam at its mid-span and the columns at their mid-heights, where inflection points are likely to occur under the lateral loads. Figs. 1 and 2 show the geometry and reinforcing details of the test specimens. The column had the same cross-dimension of 300×360 mm with a height of 3100 mm. The width of the beam was 300 mm in specimen S1-BC1, and it was increased to 450 mm in specimen S2-BC1.5. Specimens were cast at one time using a single batch of concrete. Two sizes of standard reinforcement were used for longitudinal (D16) and transverse reinforcement (D10) in all specimens. Table 1 summarises the average mechanical properties of the concrete and reinforcing bars. The concrete cylindrical strength, f'_c, was taken as 80% of the cube strength, f_{cu}.
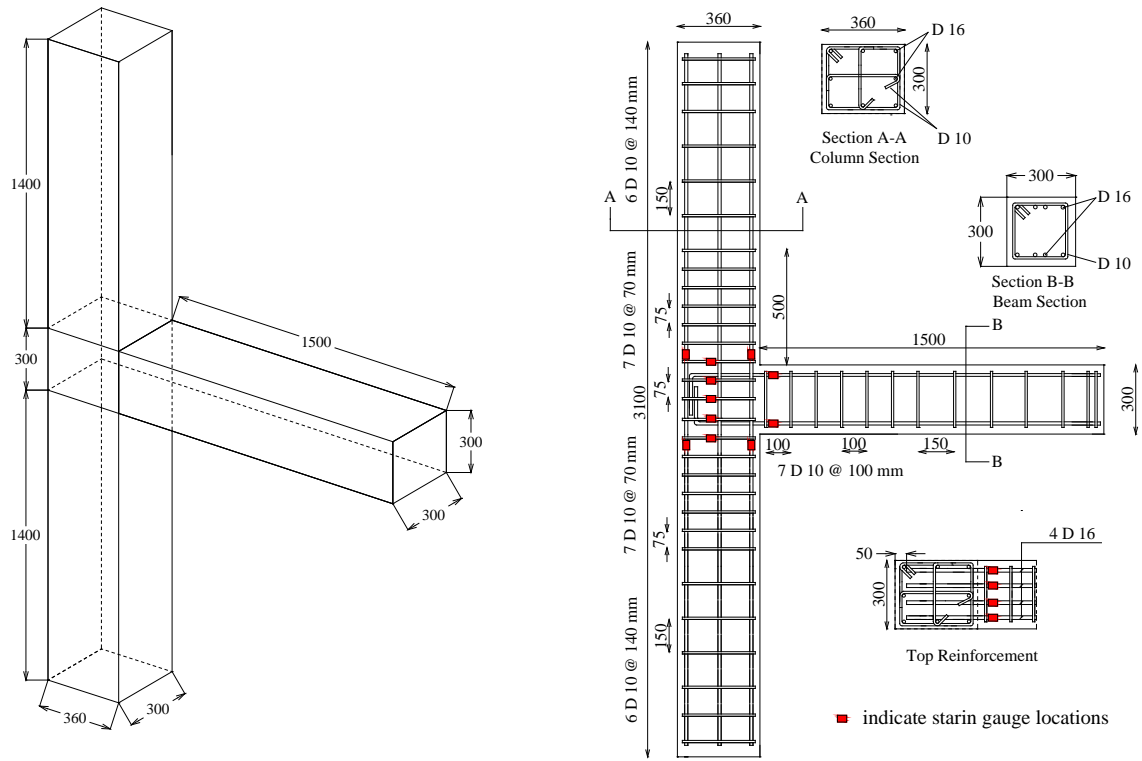
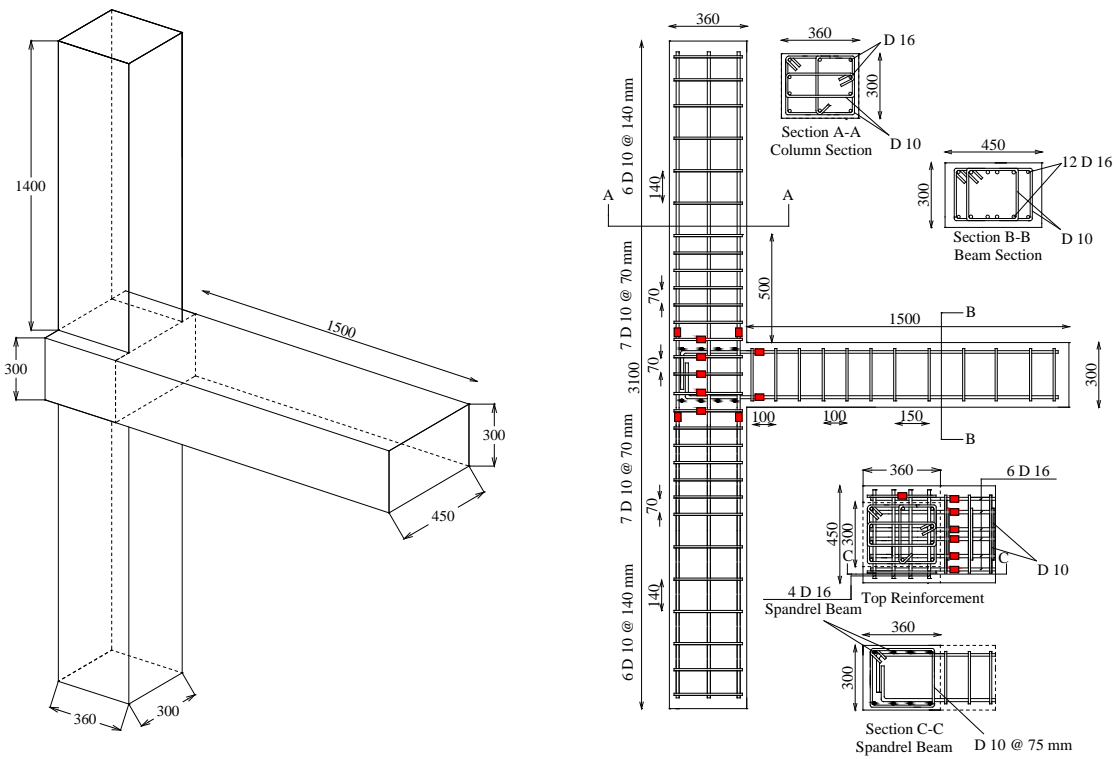Fig. 1 – Dimensions and reinforcement details of specimen S1-BC1 (unit: mm).

Fig. 2 – Dimensions and reinforcement details of specimen S2-BC1.5 (unit: mm).

3

Table 1 – Material properties of specimens

Concrete		Steel reinforcement		
f_{cu} (MPa)*	f'_c (MPa)	Bar size (mm)	f_y (MPa)	f_u (MPa)
45.2	36.1	10	485	622
* Average strength of three cubes		16	522	599

The main design parameters of the specimens, such as the column ($M_{n,c}$) and beam ($M_{n,b}$) nominal flexural capacities, column-to-beam flexural strength ratio (M_r), estimated lateral load ($V_{b,e}$), and joint shear demand ($V_{j,e}$), were estimated based on the measured properties of the materials. The specimen capacities were calculated using the actual material strength by ACI 318-14, and they are referred to as expected strengths, as summarised in Table 2.

Table 2 – Design parameters and expected capacities

Specimen	b_w/b_c	$M_{n,c}$ (kN.m)	$M_{n,b}$ (kN.m)	M_r [a]	$V_{b,e}$ (kN) [b]	$V_{j,e}$ (kN) [c]
S1-BC1	1	142	92.6	3.07	70	483
S2-BC1.5	1.5	177	138.8	2.55	105	725

[a] $M_r = \sum M_{n,c} / \sum M_{n,b} \geq 1.2$

[b] $V_{b,e} = M_{n,b} / 1.32$

[c] $V_{j,e} = 1.25 A_s f_y - V_{col}$, where A_s is the beam flexural reinforcement area and V_{col} is the column shear force.

Table 2 shows the strong column-weak beam philosophy ($M_r > 1$) was used in the design of specimens. The column-to-beam flexural strength ratios also were larger than 1.5 as suggested by ACI 352R-02. A large value of M_r in wide beam-column connections will reduce the possibility of column bars slipping through relatively shallow wide beams in the connection region. Based on the expected strength of the specimens, beam failure was expected in both specimens.

3. Test setup and measurements

The test setup is shown in Fig 3. For the convenience of applying loading and testing, each beam-column assembly was rotated 90° from the true orientation (the column positioned horizontally and the beam positioned vertically). The beam tip was linked to an actuator with a swivel connector to apply the lateral load. The beam tip and the left and right sides of the column were all pin-connected in the loading plane, to simulate the inflection points. The column pin-to-pin storey height was 2700 mm, while the beam length between the loading point and the column face was 1320 mm.

Initially, an axial load of 500 kN (12.8% of the column axial capacity) was applied to the column through a hydraulic jack positioned between the column and one of the reaction blocks, and the amount of axial force was checked from the load cell placed on another side of the column. This axial load was considered to simulate gravity. The axial load was applied in a force controlled mode and was maintained constant throughout the test. Then, the lateral cyclic displacement (Δ) was applied to the top of the beam in two opposite directions. The lateral load history consisted of several sets of three cycles with different horizontal displacements amplitudes, as shown in Fig 4. The amplitude of the cycles was constant within each set, but it increased in consecutive sets of cycles. Each cycle for a new drift level was performed three times to evaluate the loss of strength and stiffness of the specimens during repeated cycles.

Specimens were instrumented extensively by fixing strain gauges at critical locations on the reinforcement bars. The locations of the strain gauges on the longitudinal and transverse steel bars in the beam and column are shown in Figs. 1 and 2, as red colour spots. Linear variable displacement transducers (LVDTs) were used to measure the displacement at various locations on the specimen, as shown in Figs .3 and 5.
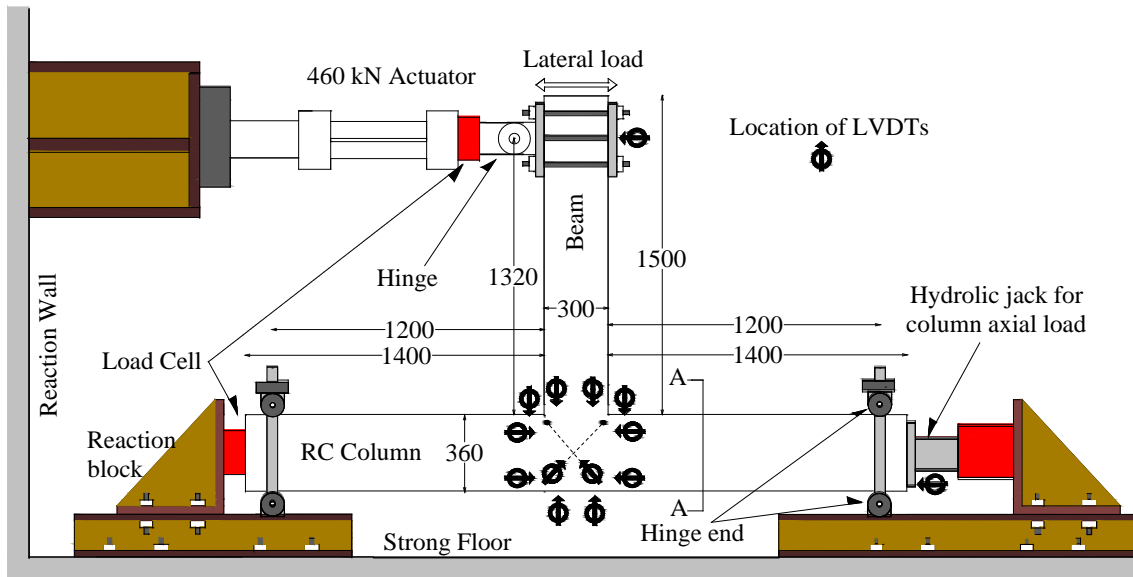
4

Fig. 3 – Schematic view of test set-up (unit: mm)
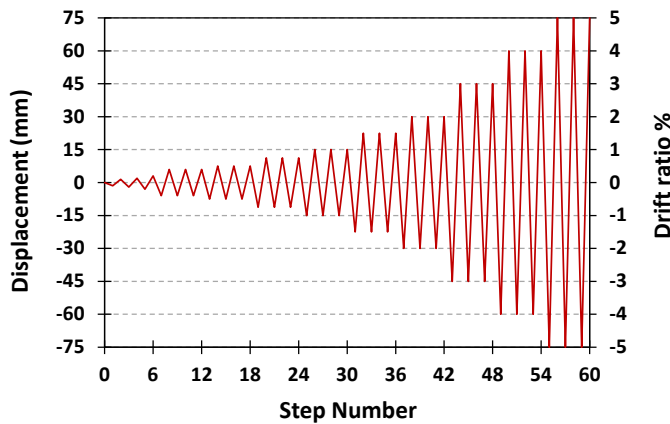

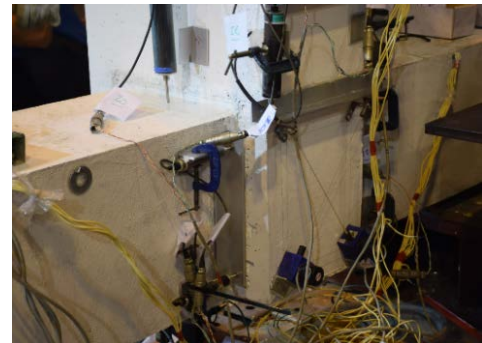Fig. 4 – Reverse cyclic-load sequence

Fig. 5 – LVDTs arrangement for S2-BC1.5

The test was paused at both the positive and negative peaks of the third cycle of each drift set to mark the cracks and to take photographs. A test report was completed at each pause to associate the observations with the manually collected data.

4. Experimental results and observations

Fig. 6 shows lateral load versus drift ratio for the specimens in the form of hysteresis curves. These figures clearly show that the theoretical capacities of the beam flexural hinging in both loading directions were attained. Specimens maintained their strength until 5% drift without any major pinching of the load-versus-drift hysteresis loops for reversed cyclic loading. After 2% drift, when beam flexural deformation dominated specimens response, the hysteresis loops became even wider, which shows the excellent energy dissipation capacity.

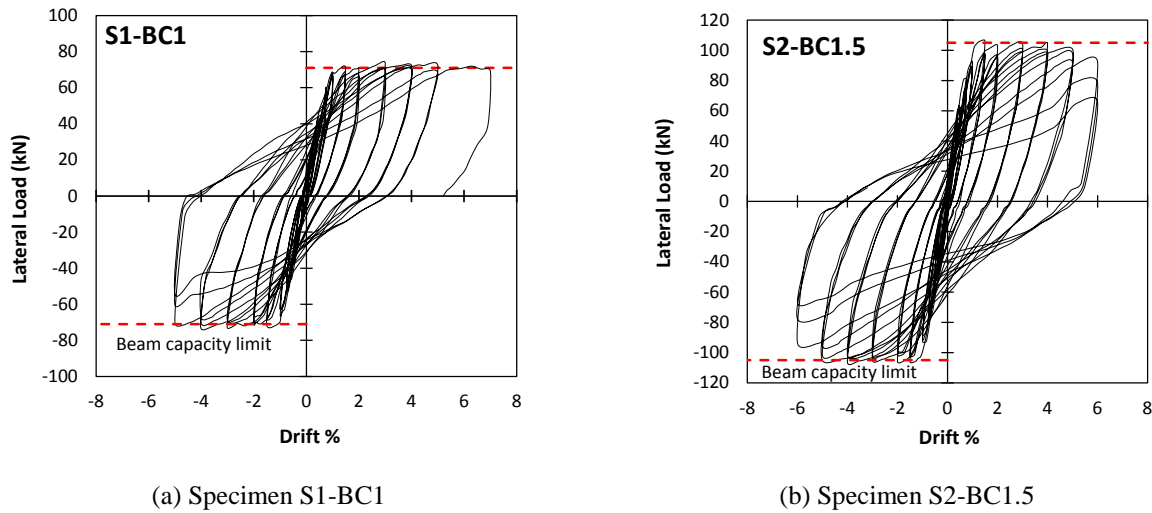(a) Specimen S1-BC1
(b) Specimen S2-BC1.5

Fig. 6 – Hysterical lateral load versus lateral drift, all specimens

The methods proposed by Lee and Ko [15] were used to identify the yielding point of specimens. According to this method, the yield displacement was determined by extrapolation from measured displacement at $0.75V_{b,e}$. Table 3 provides the relevant information for expected and maximum stiffness, strength and ductility for specimens.

Table 3 – Expected and maximum stiffness, strength and ductility

Specimen	At yielding		Initial elastic stiffness	At maximum strength		Displacement ductility
	Strength V_y (kN)	Drift (%)	K_{ini} (kN/mm)	Strength V_u (kN)	Drift (%)	
S1-BC1	-68	-1.03	4.4	-73.6	-4	4.85
	64	0.89	4.79	73.7	3	5.62
S2-BC1.5	-90	-1.00	6.00	-106.5	-4	5.00
	90	0.96	6.25	106.12	1.5	5.21

The final failure patterns of all the specimens considered in this study were obtained from repeated reverse cyclic loading, as shown in Fig 7. In specimen S1-BC1, initial flexural cracks were formed across the full width of the beam at a 0.2% drift ratio. Up to around 1% drift, the crack widths remained relatively narrow, with the specimen only having minor damage. The damage progressed at a higher rate when the drift reached a ratio of 1%. At a drift ratio of 1.5%, flexural cracks continued to develop to the full width of the beam near the beam-column interface. At 4% drift ratio, cover cracking at the beam end was observed. In specimen S2-BC1.5, the first hairline flexural crack developed in the joint interface section at a drift ratio of 0.2%. As the lateral drift increased, more flexural cracks appeared in the beam until the drift reached a ratio of 1%. In the subsequent cycles, the flexural cracks developed on a beam near the column faces. Only hairline shear (diagonal) cracks were observed on the side face of the joint during testing. Both specimens had a ductile failure mode by the formation of beam plastic hinges. It should be pointed out that in the specimen S1-BC1 the flexural cracks were mostly concentrated on the beam-column interface while in specimen S2-BC1.5, flexural cracks distributed in the expected plastic hinge region at the beam end from beam-column interface up to the 200 mm distance on the beam.

(a) S1-BC1   (b) S2-BC1.5

Fig. 7 – Crack patterns of tested specimens at 5% drift ratio

The rotational behaviour of the beams near beam/column interfaces was investigated to examine the development of beam plastic hinges. In each specimen, two LVDTs were used to estimate the total beam rotations in the vicinity of the beam/column interfaces. The LVDTs were installed on the right and left side of the beams, approximately 300 mm away from the column faces, to where a plastic hinge region might extend. Each LVDT monitored the relative displacement between the column face and the section where the LVDT was mounted. Beam rotations in the plastic hinge regions (θ_{ph}) were computed by:

$$\theta_{ph} = \frac{\Delta_{right} - \Delta_{left}}{h_{ph}} \tag{1}$$

Here h_{ph} is the horizontal distance between LVDTs on the both side of the beam (400 mm), Δ_{right} is the relative displacements measured by the LVDT on the right side of the beam, and Δ_{left} is the relative displacements measured by LVDT on the left side of the beam.
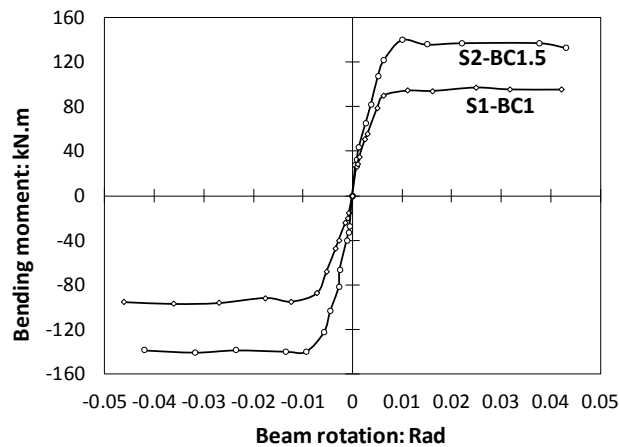

Fig. 8 – Envelope curves of beam end bending moment against beam rotation

Beam rotations were considered positive when the specimen was loaded in the positive direction. The estimated beam rotation comprised both plastic hinge rotation and rigid beam-end rotation. Plastic hinge rotation

was due to yielding of longitudinal beam bars near the interfaces after concrete cracking. The rigid beam-end rotation was attributed to a bond slip of reinforcing bars and opening of large flexural cracks at the interfaces.

Fig. 8 compares the envelope curves of bending moment against beam rotation in specimens, from connecting the peak drift point of each cycle. In general, both specimen S1-BC1 and S2-BC1.5 showed similar beam rotations throughout testing. These specimens underwent beam hinging in the plastic hinge regions. Also, beam rotation increased whereas beam moments at the beam/column interfaces did not increase during higher drift cycles. These observations imply that beam hinging had developed in the plastic hinge regions.

5. Finite element analysis

The existing test database on exterior wide beam-column connection is very limited, and it cannot address all behavioural aspects of the wide beam-column connections. Finite element model (FEM) is well known for its versatility in supplementing experimental research and providing insights into the structural behaviour of wide beam-column connections. Nonlinear three-dimensional FEM is capable of accurately modelling the mechanical properties, crack formation and propagation, deflections, and possible failure mechanisms. A finite element model (FEM) is created using the FEM package ABAQUS/Standard software. First, the procedure for calibrating the model is presented. The constitutive models for the material are described in detail. The numerical results are compared to the test results regarding deflections, strength and crack patterns. Then the finite element simulation is adopted to investigate the effect of the joint transverse reinforcement.

5.1 Material properties and constitutive models

Concrete damage plasticity (CDP) model proposed by Lubliner et al. [16] and then modified by Lee and Fenves [17] was used to model the concrete behaviour. This model assumes that the main two failure modes are tensile cracking and compressive crushing. The concrete behaviour in tension is characterised by a stress-crack displacement response, as shown in Fig. 9a, where f_t is the maximum tensile strength and G_f denotes the fracture energy of concrete that represents the area under the tensile stress-crack displacement curve. Adopting stress-crack width displacement based on the fracture energy can prevent mesh-sensitivity and allow for numerical convergence. The fracture energy of concrete G_f (N/m) for ordinary normal weight concrete can be obtained CEB-FIP Model Code 2010 [18]. The concrete stress-strain behaviour under compressive loading was modelled in three phases (Fig. 9b) using the formulations given in [19].

(a) Stress-displacement relationship under uni-axial tension

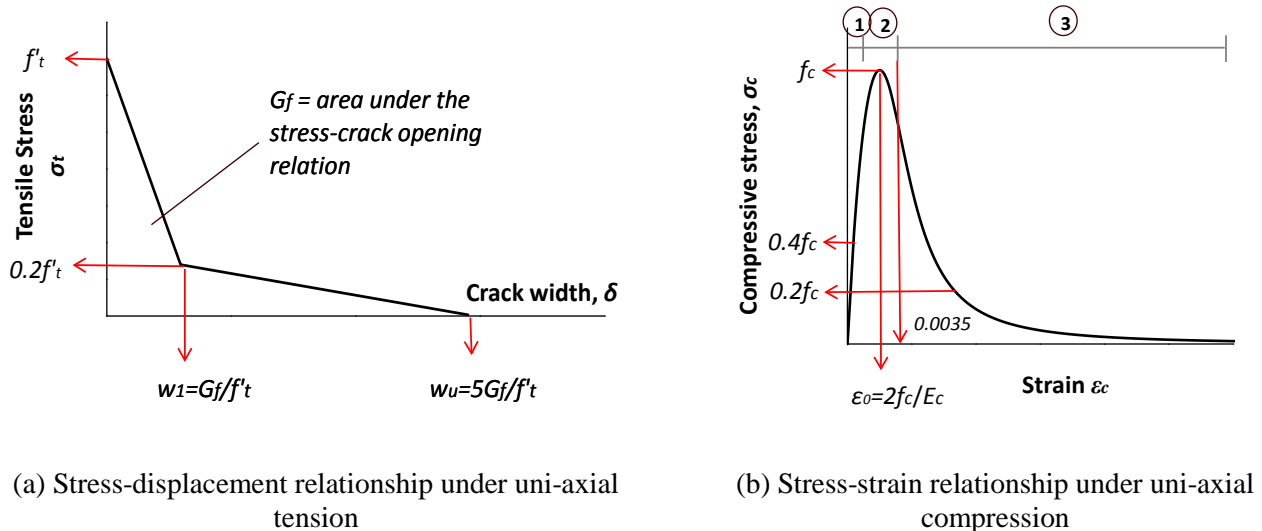(b) Stress-strain relationship under uni-axial compression

Fig. 9 – Concrete constitutive model.

Damage parameters were introduced in the CPD model in tension and compression, respectively. Concrete damage is assumed to occur in the softening range in both tension and compression. In this paper, the maximum value for the damage parameters in both tension and compression is chosen as 0.95, which corresponds to a 95% reduction of the stiffness. The choice of the damage properties is important since excessive damage may have a critical effect on the rate of convergence. The steel was assumed to be a simplified bilinear material and identical in tension and compression. The elastic modulus, E_s, and Poisson's ratio were assumed to be a 200 GPa and 0.3 respectively. Plastic behaviour was defined in a tabular form, including yield stress and corresponding plastic strain. The plastic properties were defined based on the test results with a bilinear strain hardening yield stress-plastic strain curve. The bond between the steel reinforcement and the concrete was assumed as perfect.

5.2 Numerical analysis

In the finite element models, concrete was modelled with linear 8-node, 3-D solid elements (C3D8R). The reduced integration technique, which uses a lower-order integration to form the element stiffness, was adopted to eliminate the locking behaviour resulting from the first-order elements. Longitudinal reinforcement and stirrups are modelled with linear 2-node, 3-D truss elements (T3D2) which are embedded in the concrete element. An average mesh size of 50 mm is adopted for the models. The concrete material parameters that were used in the presented analyses are: the modulus of elasticity E_c = 28250 MPa, the Poisson's ratio v = 0.2 and the compressive and tensile strengths of the concrete were considered as 36.1 MPa and 3.05 MPa respectively. The concrete damaged plasticity model considers a constant value for the Poisson ratio, v, even for cracked concrete. The dilation angle was considered as 40 degree, the shape factor, K_c = 0.667, the stress ratio = 1.16 and the eccentricity = 0.1. Damage was introduced in concrete damaged plasticity model both in tension and compression. The displacement was applied to the beam tip with small gradual increments similar to the actual test setup. Automatic stabilisation and small time increment were also used to avoid a diverged solution. Static analysis in ABAQUS/Standard with the viscosity regularisation was performed. Viscosity parameter for the static analysis was taken as 0.00001.

6. Finite element analyses results

The FEM analyses were undertaken, and the results are shown in Fig. 10 together with the experimental results. The computed stiffness, peak loads, and ductility ratios agree well with the test values. Nevertheless, the analyses indicate slightly higher initial stiffness due primarily to the micro-cracks in concrete before testing. The good agreement between test results and FEM indicates that the constitutive models used for concrete and reinforcement can capture the behaviour satisfactorily.
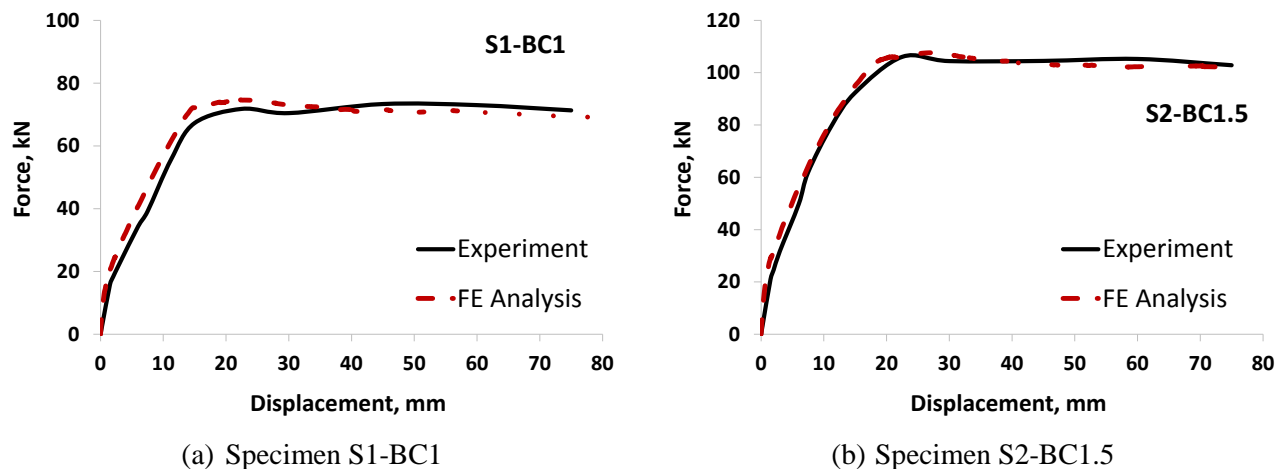

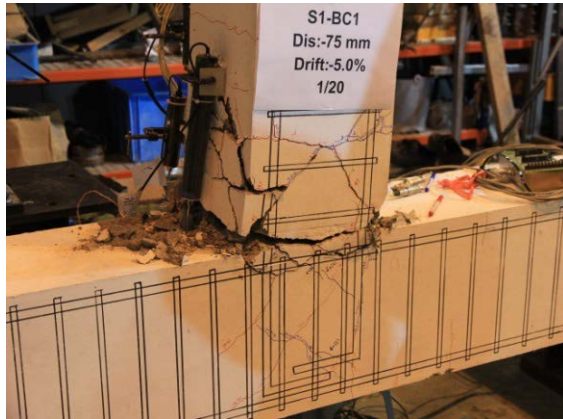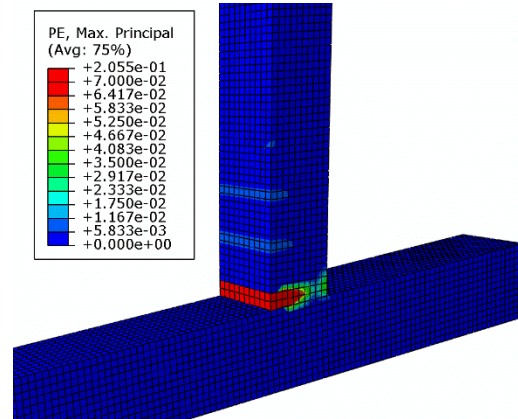(a) Specimen S1-BC1   (b) Specimen S2-BC1.5

Fig. 10 – Load-displacement skeleton curves from the experiment and numerical analysis

The cracking pattern is presented in Fig. 11. The cracking propagates inside the beam adjacent to the column. It starts near the column and then extends to the beam plastic hinge region as the load increases. At the ultimate load, the plastic hinge is visible. Concrete damaged plasticity model assumes that the cracking initiates when the maximum principal plastic strain is positive. The orientation of the cracks is considered to be perpendicular to the maximum principal plastic strains, and thus, the direction of the cracking is visualised through the maximum principal plastic strains (Fig. 11). The yielding of the flexural reinforcement has occurred at the failure in both test and FEA. Table 4 compares the experimental and numerical results regarding ultimate lateral failure load and drift ratio at the failure load.
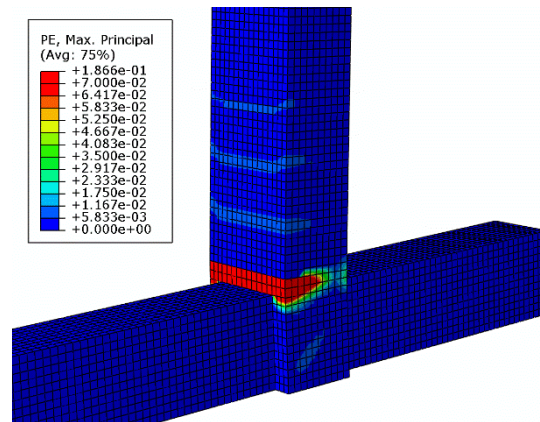

(a) Specimen S1-BC1, experiment

(b) Specimen S2-BC1.5, FEM
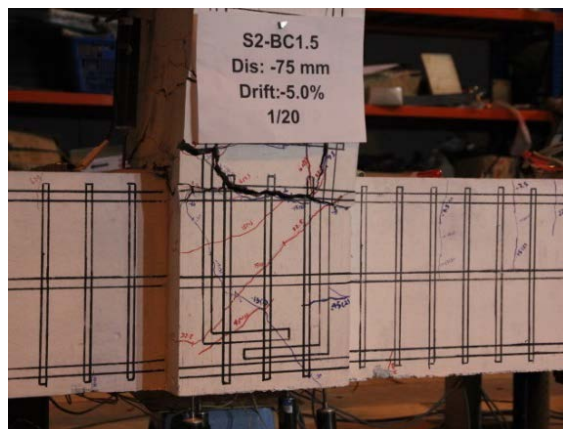
(a) Specimen S1-BC1, experiment

(b) Specimen S2-BC1.5, FEM

Fig. 11 – Cracking pattern on tension surface at ultimate load.

Table 4 –The ratio of maximum strength to expected strength and related drifts

Specimen	Test results		FEM results	
	Peak lateral load (kN)	Drift (%)	Peak lateral load (kN)	Drift (%)
S1-BC1	73.6	4	74.6	3.13
S2-BC1.5	106.5	4	107.6	3.26

It can be seen in Table 4 that the model prediction of the maximum lateral force lead to an error below 6%, which once again shows that the predictions of the FEA are in close agreement with the experimental results.

7. Effect of joint transverse reinforcement

The test specimens in this study consisted of a joint which was reinforced by transverse reinforcement. The joint contained three layers of the closed stirrup, and each layer had four legs of the D10 bars. A parametric study using a verified numerical model was carried out to investigate the effect of the transverse reinforcement on the seismic behaviour of the connections. To this end, the amount of the joint transverse reinforcement was reduced to half and zero percent of the original one. The results of the modelling are shown in Fig. 12. It can be seen that both joints perform well even with 50% of the joint transverse reinforcement. It should be pointed out the 50% transverse reinforcement was equal to three layers of the closed stirrup in which each layer had two legs of the D10 bars. However, the absent of the joint transverse reinforcement led to strength reduction and joint shear failure in both cases.
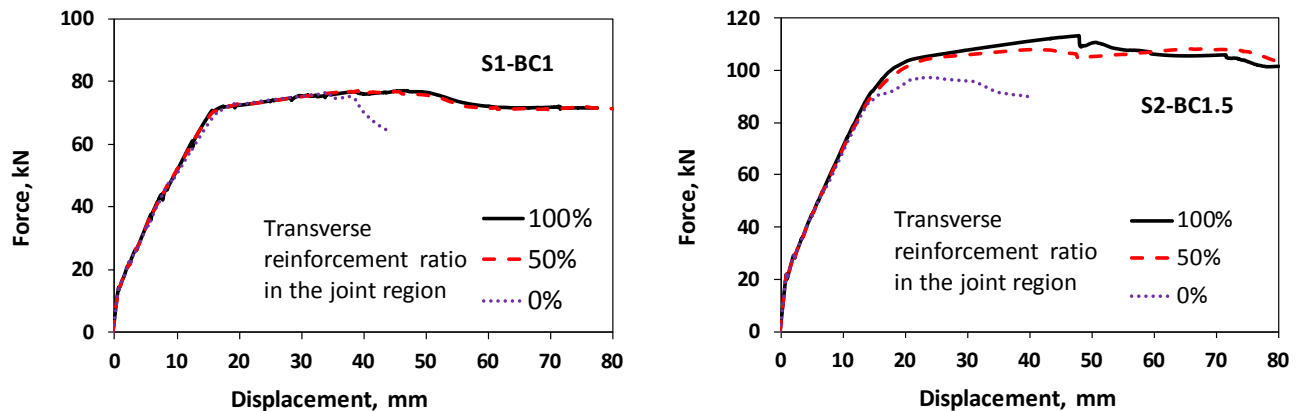

Fig. 12 – Load-displacement skeleton curves at the beam end from experiment and numerical analysis.

8. Conclusions

An experimental and numerical investigation was carried out to develop new data and to study the cyclic behaviour of wide beam-column connections. Two full-scale exterior reinforced concrete beam-column connections were tested under reversed cyclic loading. Experimental verifications showed that the wide beam-column connections designed with suitable parameters (current using ACI 318-14 and ACI 352-R02 for seismic design purposes) perform quite well in carrying horizontal lateral loads as they can attain their strength and deformation capacity. The finite element analysis with the concrete damaged plasticity model was used for predicting the response of the connections. The constitutive model has been first calibrated using experimental results of the experiments. The results of the analyses compared to the test results showed good agreement. The finite element analysis results confirm the ability of the proposed model for predicting the behaviour of the beam-column connections. The calibrated model was then used for the analyses of wide beam-column connections subjected to gravity and lateral displacements with different amount of the transverse reinforcement in the joint region. Results of the modelling showed that the absent of the joint transverse reinforcement would increase the possibility of the joint shear failure in both conventional and wide beam-column joints. The results also indicated that minimum amount of the joint transverse reinforcement recommended by ACI code is an acceptable limit in both conventional and wide beam-column joint. Providing additional joint transverse reinforcement will not change the behaviour but increase the construction difficulties of wide beam-column connections.

9. Acknowledgements

10. References

[1] Popov EP, Cohen JM, Koso-Thomas K, Kasai K (1992): Behaviour of interior narrow and wide beams. *ACI Struct. J.,* **89**(6), 607-616.

[2] LaFave JM, Wight JK (2001): Reinforced concrete wide-beam construction vs. conventional construction: resistance to lateral earthquake loads. *Earthq Spectra*, **17** (3), 479-505.

[3] Wong HF and Kuang JS (2008): Effect of beam-column depth ratio on seismic behaviour of exterior beam-column joints. *Structures and Buildings*, ICE, **161** (2), 91-101.

[4] Kitayama K, Otani S, Aoyama H (1991): Development of design criteria for RC interior beam-column joints. In: Jirsa JO, editor. Design of beam-column joints for seismic resistance, SP-123. Farmington Hills, Mich, *American Concrete Institute*, 97-123

[5] Hwang SJ, Lee HJ(1999): Analytical model for predicting shear strength of exterior reinforced concrete beam-column joints for seismic resistance. *ACI Struct J*, **96** (5), 846-858.

[6] Park H, Choi K (2007): Strength of exterior slab–column connections subjected to unbalanced moments, *Engineering Structures*, **29**(6), 1096-1114.

[7] Behnam H, Kuang JS, Huang Q (2016): Equivalent frame analysis for effective wall width of nonplanar beam-wall connections. *Struct Des Tall Spec,* DOI: 10.1002/tal.1303.

[8] Gentry TR, Wight JK (1994): Wide beam-column connections under earthquake-type loading. *Earthq Spectra,* **10**, 675-703.

[9] LaFave JM, Wight JK (1999): Reinforced concrete exterior wide beam-column-slab connections subjected to lateral earthquake loading. *ACI Struct J*, **96** (4), 577-86.

[10] Siah WL, Stehle JS, Mendis P, Goldsworthy H (2003): Interior wide beam connections subjected to lateral earthquake loading, *Eng Struct*, **25**, 281-91.

[11] Benavent A, Cahis X, Zahran R (2009): Exterior wide beam-column connections in existing RC frames subjected to lateral earthquake loads. *Eng Struct*, **31**, 1414-1424.

[12] Elsouri A, Harajli M (2013): Seismic response of exterior RC wide beam–narrow column joints: Earthquake-resistant versus as-built joints. *Eng Struct*, **57**, 394-405.

[13] Fadwa I, Ali TA, Nazih E, Sara M (2014): Reinforced concrete wide and conventional beam–column connections subjected to a lateral load. *Eng Struct*, **76**, 34-48.

[14] Behnam H, and Kuang JS (2015): Combined effect of torsional and flexural moments in wide beam-column connections. *Proc., SECED 2015 Conference: Earthquake Risk and Engineering Towards a Resilient World,* Cambridge, United Kingdom.

[15] Lee HL, Ko JW (2007): Eccentric reinforced concrete beam-column connections subjected to cyclic loading in principal directions. *ACI Struct J*, **104**, 459-467.

[16] Lubliner J, Oliver J, Oller S, Onate E (1988): A plastic-damage model for concrete. *Int J Solids Struct*, **25** (3), 299-326.

[17] Lee J, Fenves GL (1998): Plastic-damage model for cyclic loading of concrete structures. *J Eng Mech*, **124** (8), 892–900.

[18] CEB-FIB-Model Code 1990: Design Code, London: Thomas Telford, 1993.

[19] Birtel V, Mark P (2006): Parameterised finite element modelling of RC beam shear failure, *ABAQUS Users' Conference*. 95-108.